Year: 2018

Biofabricating atherosclerotic plaques: In vitro engineering of a three-dimensional human fibroatheroma model

Mallone, Anna ; Stenger, Chantal ; Von Eckardstein, Arnold ; Hoerstrup, Simon P ; Weber, Benedikt

Abstract: Atherosclerotic plaques are cholesterol-induced inflammatory niches accumulating in the vascular sub-endothelial space. Cellular and extracellular composition of human plaques is maneuvered by local inflammation that leads to alterations in the original vascular microenvironment and to the recruitment of an invading fibrous layer (fibroatharoma). In the present study we introduce a bioengineered three-dimensional model of human fibroatheroma (ps-plaque) assembled with a tailored hanging-drop protocol. Using vi-SNE based multidimensional flow cytometry data analysis we compared the myeloid cell-populations in ps-plaques to those in plaques isolated from human carotid arteries. We observed that plasmacytoid and activated dendritic cells are the main myeloid components of human carotid plaques and that both cell types are present in the biofabricated model. We found that low-density lipoproteins affect cell viability and contribute to population polarization in ps-plaques. The current work describes the first human bioengineered in vitro model of late atherosclerotic lesion for the investigation of atherosclerosis aetiopathogenesis.

Biofabricating atherosclerotic plaques: *In vitro* engineering of a three-dimensional human fibroatheroma model

Anna Mallone [a, *], Chantal Stenger [a], Arnold Von Eckardstein [b], Simon P. Hoerstrup [a], Benedikt Weber [a]

[a] *Institute for Regenerative Medicine (IREM), University of Zurich, Zurich, Switzerland*
[b] *Institute of Clinical Chemistry, University Hospital Zurich, Zurich, Switzerland*

ABSTRACT

Atherosclerotic plaques are cholesterol-induced inflammatory niches accumulating in the vascular sub-endothelial space. Cellular and extracellular composition of human plaques is maneuvered by local inflammation that leads to alterations in the original vascular microenvironment and to the recruitment of an invading fibrous layer (fibroatharoma). In the present study we introduce a bioengineered three-dimensional model of human fibroatheroma (ps-plaque) assembled with a tailored hanging-drop protocol. Using vi-SNE based multidimensional flow cytometry data analysis we compared the myeloid cell-populations in ps-plaques to those in plaques isolated from human carotid arteries. We observed that plasmacytoid and activated dendritic cells are the main myeloid components of human carotid plaques and that both cell types are present in the biofabricated model. We found that low-density lipoproteins affect cell viability and contribute to population polarization in ps-plaques. The current work describes the first human bioengineered *in vitro* model of late atherosclerotic lesion for the investigation of atherosclerosis aetiopathogenesis.

© 2017 The Authors. Published by Elsevier Ltd. This is an open access article under the CC BY-NC-ND license (http://creativecommons.org/licenses/by-nc-nd/4.0/).

1. Introduction

Atherosclerosis is a life threatening vascular pathology characterized by the accumulation of a fatty plaque in the vascular sub-endothelial space [1]. Atherosclerotic plaque formation is influenced by the synergistic interplay of different risk factors such as sex, age, genetic predisposition, high blood pressure and high blood levels of low-density lipoprotein (LDL) cholesterol [2,3]. The formation of a well-structured plaque microenvironment results from the interplay of cholesterol-rich lipoproteins, endothelial cells, monocytes, macrophages, dendritic cells and fibroblasts in a complex matrix milieu [4]. The process of plaque formation is progressive and reversible [3,5] and can be counteracted by a reduction of the modifiable risk factors mentioned above or promoted by their persistence. Plaques are classified according to their stage of development and cellular components [4]. Among different plaque stages, the thin-cap fibroatheroma is the one most prone to rupture

and to potentially cause thrombus formation and vessel obstruction [6]. The fibroatheroma is characterized by the presence of a necrotic core, macrophage-derived foam cells and dendritic cells all being enriched with cholesterol and embedded in a collagenous matrix surrounded by a thin layer of fibrotic cells [4,5]. The cellular mechanisms underlying plaque formation and regression have been investigated *in vivo* in both small and large animals, predominantly in hypercholesterolemic mice with knock-out of either Apoe or LDL-receptor [7–9] or non-human primates [10,11]. Despite the stunning contribution to the field, major differences in anatomy, lipoprotein profiles and inflammatory mechanisms hampered the translation of these results to the human pathophysiology. To overcome the translational gap, human cell-based co-culture *in vitro* models have been established and provided a first glimpse into the initial events of plaque deposition in humans [12–15]. To our knowledge, no human model of late stages of atherosclerotic plaque development does exist. In the present study we introduce a bioengineered *in vitro* model of fibroatheroma that we call pseudo plaque (ps-plaque). The ps-plaque architecture is characterized by a spheroid core of monocytes, macrophages and dendritic cells embedded in a collagenous and lipid-rich matrix, surrounded by a thin layer of myofibroblasts. In order to investigate

* Corresponding author. Institute for Regenerative Medicine (IREM), University of Zurich, Wagistrasse 12, WAD M180, Schlieren, Zurich CH-8952, Switzerland.
  E-mail address: anna.mallone@irem.uzh.ch (A. Mallone).

a possible source for model up-scaling we biofabricated ps-plaques using either blood-derived myeloid cells or cells from the thp-1 cell line. We explored the similarities in surface antigen expression patterns of myeloid populations from ps-plaques and human carotid plaques isolated from patients undergoing carotid endarterectomy. Additionally, we compared the expression levels of key pro-inflammatory and remodeling gene-targets in both plaque types. We found similarities in population distribution and gene expression profiles between ps-plaques and human samples. Finally, we used the ps-plaque to investigate the role of LDL in plaque population remodeling and cell viability. With this work we introduce a new technology for investigating atherosclerosis pathomechanisms, aiming at providing a novel human cell-based platform for drug design and high-throughput screening.

2. Materials and methods

2.1. Isolation of myeloid cells from blood

Myeloid cells were isolated from human blood using a double gradient centrifugation. The blood was provided by the Zurich blood bank (Blutspende Zürich — Nr.6676) and maintained at room temperature in slow rocking motion until processing. First, 20 ml of blood from each donor were diluted 1:2 with 1 × Phosphate Buffer Saline (PBS, Sigma) at room temperature and layered onto a Ficoll solution (1.077 g/ml, Sigma). Samples were then centrifuged at 400 g for 30 min without break. Second, a 46% iso-osmotic Percoll gradient was performed to separate the lymphocytes from the peripheral blood mononuclear cells (PBMCs) as previously described [16]. Briefly, the buffy coat was re-suspended in 20 ml of xVivo15 chemically defined medium (Lonza) without red phenol and carefully layered on top of a Percoll solution prepared with 50% Roswell Park Memorial Institute (RPMI) medium with red phenol (Sigma), 46% Percoll (GE Healthcare) and 4% 1 × PBS (Sigma). The second gradient was centrifuged at 550 g for 30 min without break and the white cell ring at the interphase was collected for further processing.

2.2. Myofibroblasts isolation

Human umbilical vein myofibrobalsts (HUVM) were isolated from human umbilical cords. The tissues were processed in accordance to the ethical permit released by the Kantonale Ethikkommission Zürich (KEK-Stv-21-2006). Briefly, umbilical cords were stored after labor at 4 °C in Dulbecco's Modified Eagle's Medium (DMEM, Sigma) prepared with 10% Fetal Bovine Serum (FBS, Gibco), 1% GlutaMax (Gibco) and 1% penicillin/streptomycin (Penn/Strep, Gibco) for maximum 2 h prior to processing. The umbilical vein was carefully extracted from the umbilical cord and the inner lumen was flashed twice with 1 × PBS. The adventitia layer was peeled off with the help of forceps and scalpel. The intima layer was removed by incubating the inner lumen for 30 min in a 1 mg/ml collagenase/dispase (Roche) solution in 1 × PBS. The remaining endothelial cells were washed out from the lumen with 1 × PBS. The remaining media layer was minced into small pieces of approximately 2 mm length and let adhere for 10 min on the bottom of a petri dish. The tunica media fragments were then covered in DMEM medium and maintained at 37 °C, 5% CO_2 and 95% humidity. The medium was replaced every 48 h. After about 20 days myofibroblasts sprouting from the minced pieces reached about 80% confluence and were ready for sub-culturing.

2.3. Cell culture

HUVM were cultured in DMEM medium with 10% FBS and 1%

GlutaMax and the medium was replaced every 48–72 h. For subculturing, HUVM were detached using trypsin 0.5% (Sigma) for 4 min and seeded at a cell density of 4000 cells/cm². HUVM were expanded up to passage 5 prior to use for the experiments in this study. Human monocytic leukaemia cell line (thp-1) isolated from the peripheral blood of a 1-year-old human male with acute monocytic leukemia, were purchased from Sigma. Thp-1 cells were cultured in suspension in xVivo15 medium and the medium was replaced every 2–3 days. Thp-1 cells were seeded at a density of 100,000 cells/ml and sub-cultured at a density of 800,000 cells/ml.

2.4. Ps-plaque biofabrication

The pseudo-plaque production pipeline encompasses three steps: differentiation, priming and hanging-drop. First, fresh blood-derived myeloid cells or thp-1 cells were seeded onto petri dishes for 72 h and differentiated in chemically defined xVivo15 medium with 10% FBS in order to achieve a macrophage/dendritic cell phenotype. To induce thp-1 differentiation 10 ng/ml of phorbol 12-myristate 13-acetate (PMA, Sigma) were added to the culture medium. Second, a priming step was performed to obtain heterogeneous macrophage/dendritic cell populations with both pro-inflammatory and remodeling phenotypes. For this purpose the differentiated cells were rinsed in 1 × PBS and treated for 1 h in xVivo15 medium with 10% FBS and 10 ng/ml lipopolysaccharide (LPS, Sigma). Finally, the primed cells were transferred in hanging-drop culture. Briefly, adhesive myeloid-derived cells were mechanically detached by 20 min incubation in 5 mM Ethylenediaminetetraacetic acid (EDTA, Life Technologies) in 1 × PBS at 4 °C and gentle scraping. Cells were re-suspended at a cell density of 2.4×10^6 cells/ml in presence of LDL 50 µg/ml (LEE Biosolutions) in xVivo15 medium with 10% FBS. Droplets of 10 µl were pipetted on the lead of a 10 cm diameter petri dish and kept in hanging-drop culture for 48 h. To the core of myeloid-derived cells assembled during the 48 h incubation, an external layer of HUVM was added. HUVM were prepared at a cell density of 4×10^5 cells/ml in DMEM medium, with or without 50 µg/ml LDL. 10 µl of the cell suspension were carefully added to each pre-existing drop and cultured in hanging-drop for further 48 h.

2.5. 2D co-culture

Primed myeloid cells from blood or thp-1 origin were seeded in 24 well plates maintaining the same cell ratio used for the ps-plaque biofabrication (myeloid cells:myofibroblasts 6:1). In detail, about 300′000 primed myeloid cells were seeded with or without 50 µg/ml LDL in each well in order to achieve a confluent cell layer. Cells were kept in xVivo15 medium with 10% FCS and in 2D culture for 48 h. 50′000 fibroblasts/well in DMEM medium (with or without 50 µg/ml LDL) were then added on top of the myeloid cell layer and incubated for 48 h to obtain a stratified 2D co-culture system.

2.6. Flow cytometry

Biopsies of carotid branches were obtained from patients undergoing carotid endarterectomy and shunting, secondary to vascular stenosis (Ethik Kommission der Universität Witten/Herdecke — Nr.79/2012). Carotid plaques and biofabricated ps-plaques were digested with 1 mg/ml collagenase/dispase solution in 1 × PBS for 15 min at 37 °C. Cells were gently pipetted through a cell strainer with the mesh size of 40 µm (Falcon) and incubated for 5 min at 4 °C with magnetic beads coated with anti CD45 antibodies, according to the provider instructions (MACS Miltenyi Biotec). CD45 + cells were magnetically sorted and stained with

Zombie Aqua™ fixable viability kit (BioLegend) for 5min and fixed over night at 4 °C in a 1% Paraformaldehyde (PFA, Sigma) solution in $1 \times$ PBS. The single cell suspension was stained for 15 min at room temperature in Fluorescence-activated cell sorting (FACS) buffer prepared with 5% FBS and 0.01% NaN$_3$ (Sigma) in $1 \times$ PBS with an optimized FACS antibody panel including: CD14-PerCP (#325631, Biolegend), CD16-Alexa 700 (#360717, Biolegend), CD11b-Alexa594 (#101254, Bioloegend), CD11c-PE-Cy5 (#301609, Biolegend), CD36-BV605 (#563518, Becton Dickinson) and SRA-1-PE (#REA460, MACS Miltenyi Biotec). Each antibody was previously titrated to establish the optimal working concentration. Samples were acquired using LSR Fortessa analyzer (Becton Dickinson) and signal compensation was performed using OneComp eBeads (eBioscience).

2.7. vi-SNE workflow

The Flow Cytometry Standard (FCS) files obtained from the FACS analysis were pre-processed using the software Flowjo (FlowJo, LLC). First, the cell populations of interest were gated according to forward and side scatter parameters (FSC and SSC). Second, singlets and Zombie Aqua™ dye negative events were selected, representing the living cell population of interest. Data post-processing was performed using the R platform and the Cytofkit package. Briefly, pre-processed FCS files from each sample were loaded onto Cytofkit, randomly down-sampled to 2000 events (ceil; n = 2000) and computed using t-Distributed Stochastic Neighbor Embedding (t-SNE) algorithm [17]. Each event recorded was positioned in a specific location of the high-dimensional space. The output was a vi-SNE biaxial plot where distances between events are representatives of cell proximity in high-dimensional rather than two-dimensional space. The proximity between events is based on similarities in surface marker expression levels. Different myeloid subsets were positioned in separate regions in high-dimensional space according to surface marker similarities. Automatic gating of myeloid subsets was performed through a preliminary clustering step with PhenoGraph algorithm (k = 42) and a following meta-clustering step with FlowSOM algorithm (k = 10). The output of the above-described vi-SNE workflow is a vi-SNE map for each sample originally analyzed using FACS. Different biological replicates from each sample are combined to obtain a cumulative vi-SNE map.

2.8. Immunofluorescence

Myofibroblasts were fixed for 20min in 4% PFA in $1 \times$ PBS and maintained in $1 \times$ PBS at 4 °C until further processing and not more than 7 days. Cells were stained with the primary antibodies anti-alpha smooth muscle actin (αSMA, #ab7817, Abcam) and anti-smooth muscle myosin heavy chain (SMMHC, #ab53219, Abcam) overnight at 4 °C and with secondary antibodies (anti-mouse #715-605-151, Jackson Immuno Research; anti-rabbit #A11008, Life Technologies) and phalloidin (#A12381, Life technologies) for 1 h at 37 °C. Nuclei were counterstained with DAPI and the slides were mounted in Vectaschield® (Vector Laboratories). The ps-plaques were carefully washed in $1 \times$ PBS and fixed in PFA as described above. Plaques were dehydrated overnight in a solution of 25% sucrose (Sigma) in $1 \times$ PBS, embedded in OCT matrix (CellPath) and stored at −20 °C. Slices of 5 μm were cut, rehydrated in $1 \times$ PBS for 15min and stained with primary antibodies: anti-Collagen type III (#ab7778, Abcam), anti-αSMA and anti-CD45-PeCy5 (#304009, BioLegend) overnight at 4 °C. Secondary antibody staining was performed (anti-mouse, 715-545-151, Jackson Immuno Research; anti-rabbit #A11008, Life Technologies) for 1 h at 37 °C. For the Filippin sections were quenched for 10min with 1.5 mg/ml glycine (Sigma) in $1 \times$ PBS prior to addition of 250 μg/ml Filippin III dye

(Sigma) at room temperature for 2 h. Sections were washed 3 times in $1 \times$ PBS and nuclei were counterstained with propidium iodide 1 mg/ml (BioLegend) for 5min. Slides were mounted in Vecta-schield®. Images were acquired in grey scale with the confocal microscope (Leica SP8). Image post-processing, specifically the choice of appropriate pseudo-colors, was performed using ImageJ.

2.9. RT-qPCR

Total RNA was extracted using the GenElute Mammalian Total RNA Kit (Sigma), following the manufacturer's instructions. Reverse transcription was performed for each sample in a 20 μl reaction mixture containing 1 μg of RNA, $1 \times$ PCR buffer, 5 mM MgCl$_2$, 10 mM of each dNTP, 0.625 μM oligo d(T)$_{16}$, 1.875 μM random hexamers, 20U RNase inhibitor and 50U MuLV reverse transcriptase (all from Life Technologies). The conditions for the reverse transcription were the following: 25 °C for 10min, 42 °C for 1 h, followed by 99 °C for 5min. The resulting cDNA was amplified in duplicate by quantitative real-time PCR in 10 μl reaction mixture with 200 nM of each specific primer (Supplementary Table 2) and $1 \times$ Fast Syber Green qPCR MasterMix (Applied Biosystems). For the amplification reaction, StudioQuant 7 was used (Applied Biosystem). The amplification program was set as follows: 95 °C for 5min, followed by 40 cycles at 95 °C for 10 s, 60 °C for 15 s, 72 °C for 20 s. GAPDH and 18S served as housekeeping genes and their amplification data were averaged and used for sample normalization. The software Excel (Microsoft) was used for the comparative quantification analysis.

2.10. Ps-plaque viability assay

Cell viability within the plaque was measured using CellTiter-Glo® 3D Cell Viability Assay (Promega). Briefly, the biofabricated plaques were washed in $1 \times$ PBS and dispensed in a opaque-walled 96 well plate (Costar). Each ps-plaque (1 plaque/well) was dispensed in 15 μl of $1 \times$ PBS. Equal volume of CellTiter-Glo® 3D Reagent was added to each well for a final volume of 30 μl. Luminescence was measured after a 30min of incubation at room temperature with SPECTRAmax® Gemini-XS (Bucher biotech) and ATP levels were reported in relative luminescence units (RLU).

2.11. Quantification of ps-plaque area and necrotic area

For the measure of the plaque necrotic area, every plaque was stained for 40min in a solution of calcein (5 μM) and eth-1 (15 μM) from the LIVE/DEAD™ Viability/Cytotoxicity Kit, for mammalian cells (Life Technologies). Ps-plaques were imaged using an inverted microscope (Leica, DM IL LED) and post-processed in ImageJ. Briefly, images underwent color 2D Parallel iterative deconvolution using the Wiener Filter Preconditioned Landweber (WPL) method (Max number of iteration = 5; Max number of threads^2 = 4). The results of the point of spread function obtained from the deconvolution were normalized and the green and red channels were thresholded with the MaxEntropy setting. The ps-plaque necrotic area was measured as necrotic area over alive area and indicated as percentage. Plaque dimension was measured using the bright field images of the plaque circular cross section. First, the image was converted to 8-bit format and thresholded with the MaxEntropy method. Second, the area of the particles was analyzed from objects with a dimension larger than 1,000px in order to exclude debris or single cells not belonging to the bioengineered plaque. Plaque area was reported in mm^2.

2.12. Statistical analysis

vi-SNE cluster counts and PCR comparative quantitations were analyzed using multiple comparison analysis. First, Gaussian distribution of the data was confirmed with Shapiro-Wilk normality test. Second, repeated measures (RM) two-way ANOVA with Tukey's multiple comparison test was applied. Luminescence and necrotic area were analyzed with paired t-test. All statistical analyses were performed with GraphPad Prism Version 7, GraphPad Software, San Diego, CA, USA). Significance was accepted at $p < 0.05$. All data are presented as mean $\pm$ s.d..
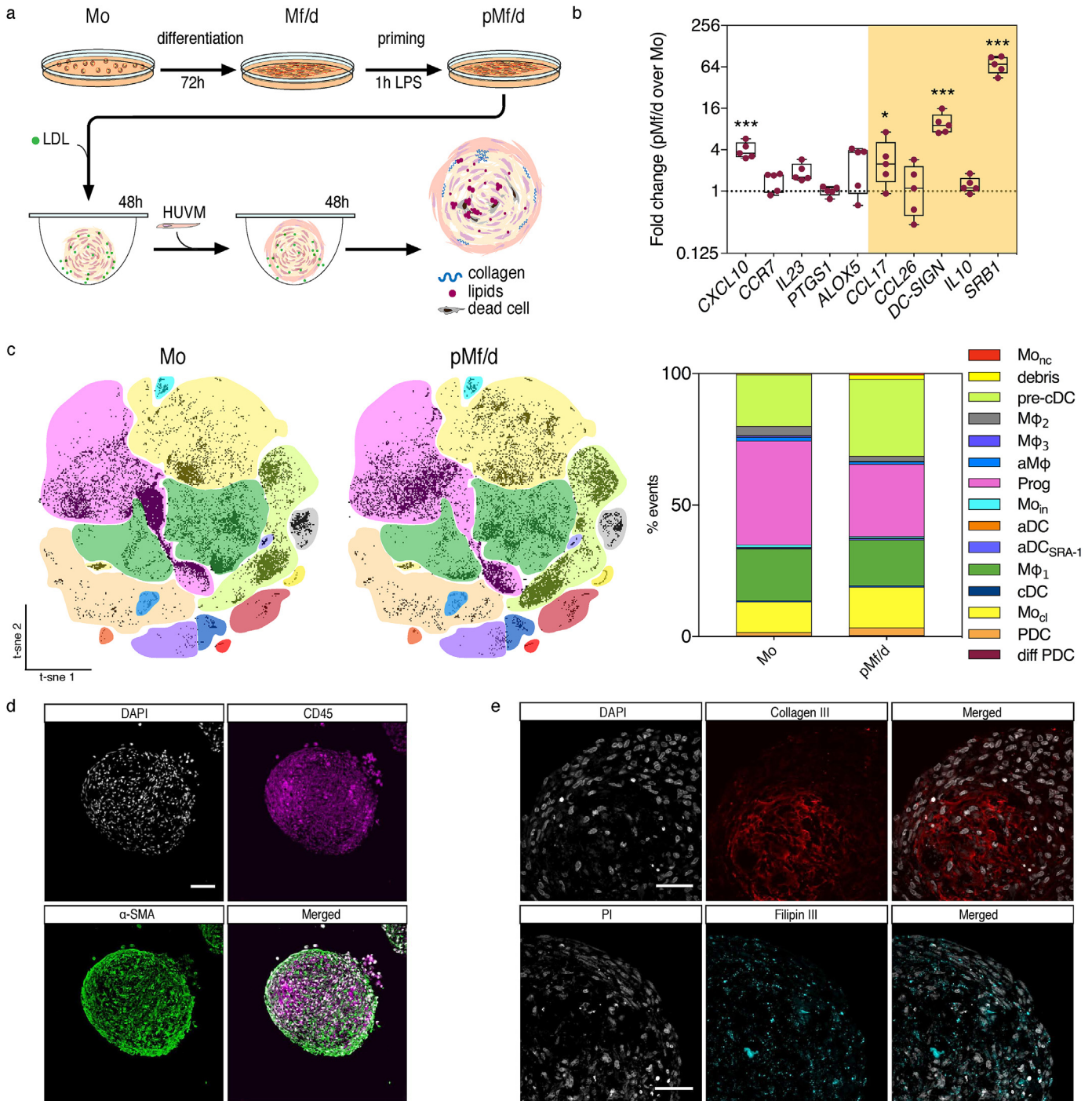

Fig. 1. Biofabricated human atherosclerotic plaque. (**a**) Schematic view of the ps-plaque assembly with blood-derived cells. (**b**) Expression profile of pro-inflammatory (left-white panel) and remodeling genes (right-orange panel) over the differentiation-priming process. Data are reported in fold change over gene expression levels at the beginning of the differentiation-priming process. N = 5; error bars indicate standard deviation; *p = 0.05, ***p < 0.001. (**c**) vi-SNE maps indicating the cell populations at the beginning (Mo) and at the end (pMf/d) of the differentiation-priming process. N = 7; 2000 events per sample are reported; 14,000 events are shown in each vi-SNE map. The stacked-bar chart indicates the percentage of events recorded in each population and summarizes the vi-SNE results. (**d**) Representative cross-section captured at the great circle of the spheroid showing inner architecture of the ps-plaque: HUVM (αSMA+, green) and myeloid cells (CD45+, magenta). Scale bar 100 μm. (**e**) Collagen III and lipid accumulation in the ps-plaque. Scale bar 50 μm.

3. Results

3.1. Differentiation-priming strategy promotes population redistribution in cells from myeloid origin

We established a two-step bioengineering method for the assembly of the ps-plaque (Fig. 1a). Myeloid cells isolated from freshly drawn blood and thp-1 cells were differentiated towards macrophage/dendritic phenotype and primed with LPS to obtain a mixed population of pro-inflammatory and remodeling cell populations. The success of the differentiation-priming strategy was verified using a fluorescence-activated cell sorting (FACS) and the results were computed using dimensionality reduction and clustering algorithms, PhenoGraph and FlowSOM respectively [18]. With this technique we identified 15 cell populations in the multidimensional space that we classified according to the differential expression levels of key surface markers (Fig. 1c; Supplementary

Fig. 1; Supplementary Fig. 2 and Supplementary Table 1). In samples isolated from the blood we identified 4 over-represented populations: classical monocytes (Mo_{cl}), macrophages ($M\varphi_1$), pre-classical dendritic cells (pre-cDC) and an unknown myeloid progenitor population (Prog) (Fig. 1c; Supplementary Fig. 2). We monitored each population at the end of the differentiation-priming process and we observed a significant decrease in the unknown myeloid progenitors (p = 0.005) coupled with a significant increase in pre-cDC (p = 0.05) (Fig. 1c). Additionally, we observed a priming-induced increase in CD11c surface levels within the pre-cDC population and in the myeloid progenitors (Supplementary Fig. 3, Supplementary Fig. 4). In cell samples from untreated thp-1 we observed an initial population distribution similar to the one found in blood samples. When we applied the priming process to thp-1 monocytes, we observed a significant reduction in the myeloid progenitors count (p < 0.001). The latter was concomitant with a decrease in pre-cDC count (p < 0.001) and
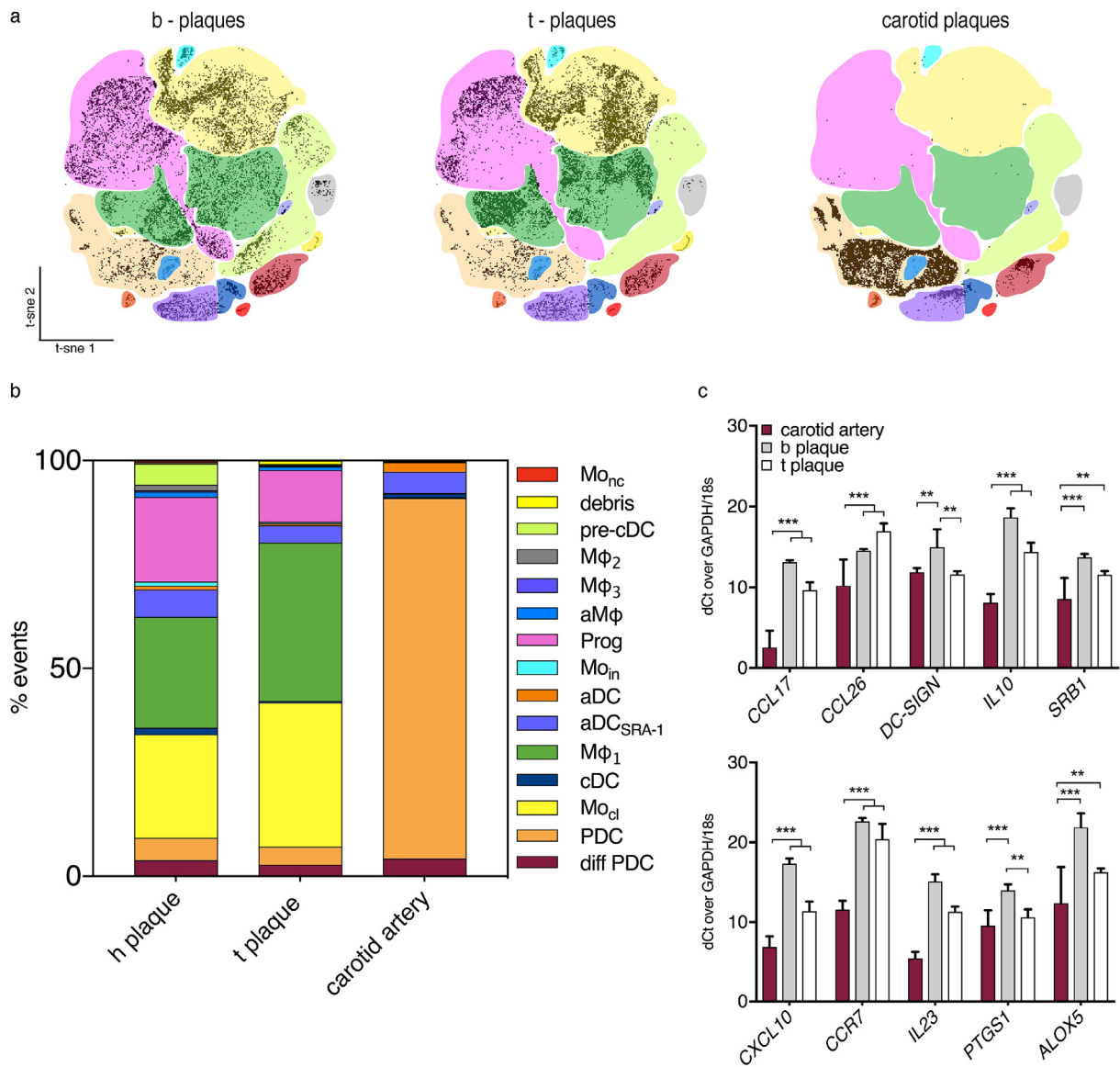

Fig. 2. Comparison between biofabricated plaques and human carotid plaques. (a) vi-SNE maps from CD45 + populations isolated from blood-derived plaques (b-plaques), thp1 plaques (t-plaques) and carotid plaques. N = 7; 2000 events per sample are reported. A total of 14,000 events are shown in each vi-SNE map. (b) The stacked-bar chart summarizes the percentage of events for each population. (c) Gene expression profile of CD45 + populations isolated from ps-plaques and plaques from carotid arteries. Expression levels of remodeling genes (upper panel) and pro-inflammatory genes (lower panel). N = 5, error bars indicate standard deviation. **p = 0.002, ***p < 0.001.

the appearance of plasmacytoid dendritic cells (PDC) (Supplementary Fig. 5, Supplementary Fig. 6, Supplementary Fig. 7). Furthermore, we observed that the priming process triggered the proliferation of classical monocytes (p < 0.001) (Supplementary Fig. 5). We then analyzed the expression levels of pro-inflammatory and remodeling gene targets. In blood derived cells we observed induction of *CXCL10* (p < 0.001), *CCL17* (p < 0.05), *DC-SIGN* (p < 0.001) and *SRB1* (p < 0.001) upon treatment, indicating the overall stronger induction of remodeling over pro-inflammatory genes (Fig. 1b). When we analyzed the changes in thp-1 cells gene expression levels upon differentiation-priming we observed induction of *CXCL10* (p = 0.03), *PTGS1* (p = 0.05) and *IL10* (p = 0.01), indicating pro-inflammatory gene up-regulation over remodeling genes (Supplementary Fig. 8).

3.2. Defining the gravity-guided biofabrication of human atherosclerotic plaques

Human primed myeloid cells and myofibroblasts (HUVM) were combined to establish a hanging-drop 3D co-culture system (Fig. 1a; Supplementary Fig. 9). The newly established system resulted in α-SMA + HUVM cells surrounding pre-existing myeloid CD45 $^+$ cell aggregates and forming a thin fibrotic layer around the bioengineered spheroid (Fig. 1d). The generation of such stratified structure and compact HUVM layer was not observed in 2D co-culture systems when using the same cell-to-cell ratio (Supplementary Fig. 10). Additionally, we observed the assembly of collagen clumps within the ps-plaque and intra-plaque accumulation of lipid aggregates (Fig. 1e). We did not detect any extracellular collagen deposition in 2D co-culture systems. Collagen was rather retained in the intracellular space (Supplementary Fig. 10).

3.3. vi-SNE analysis reveals plasmacytoid and activated dendritic cells as main myeloid components in human fibroatheroma

To corroborate the ps-plaque model we conducted a comparison study between bioengineered and human atherosclerotic plaques isolated from patients that underwent carotid endarterectomy. We
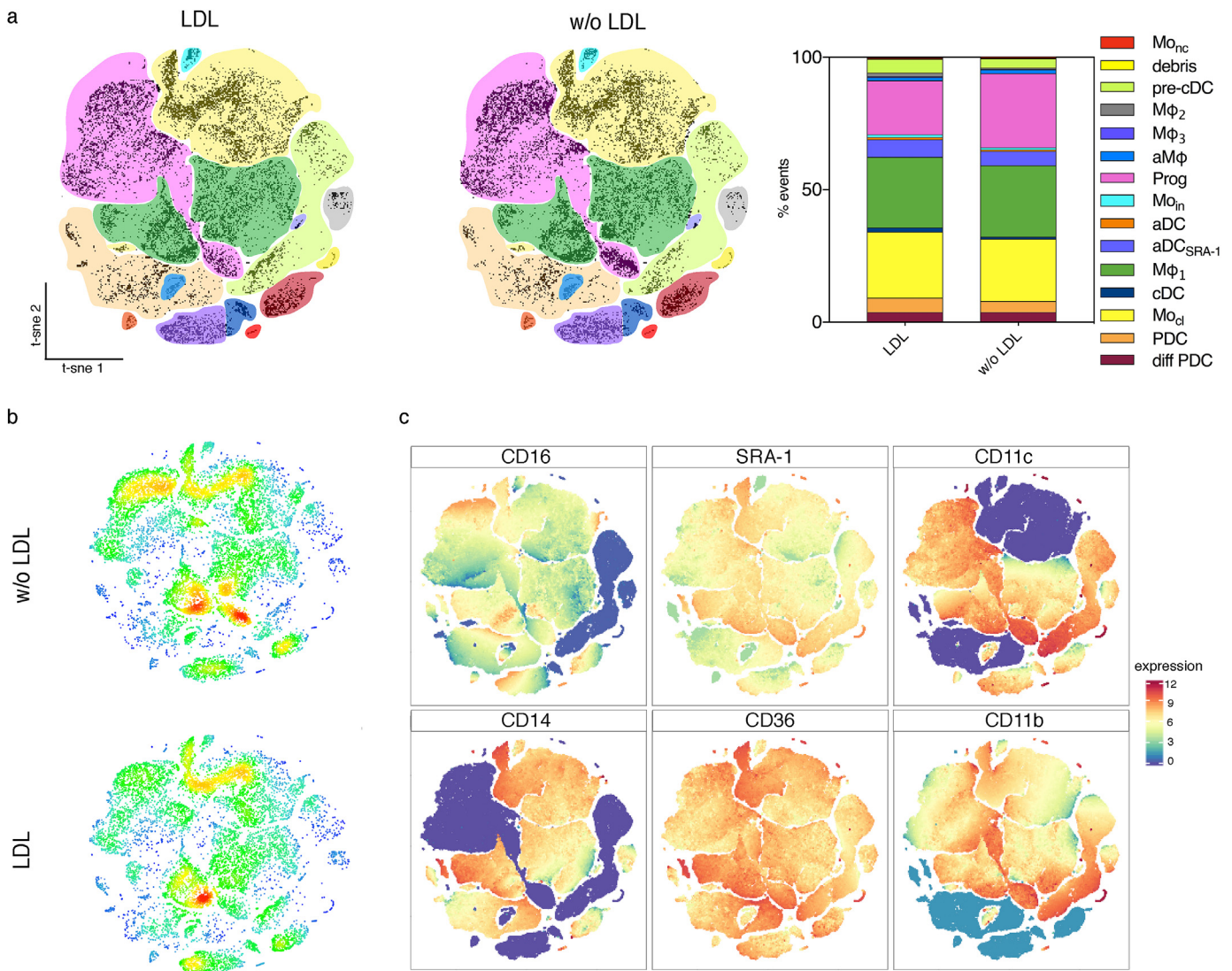

Fig. 3. LDL effects on myeloid cells isolated from b-plaques. (**a**) vi-SNE maps indicating myeloid populations identified within b-plaques biofabricated either using LDL-enriched (LDL) or LDL-free (w/o LDL) medium. The stacked-bar chart summarizes the results from the vi-SNE maps and reports the percentage of events recorded in each population. (**b**) Event density distribution vi-SNE maps show high-density (red) and low-density of events (blue) areas. (**c**) Marker expression level vi-SNE plots. N = 7; 2000 events per sample are reported; 14,000 events are displayed in the vi-SNE maps in **a** and **b**. vi-SNE maps in **c** are generated using 2000 events from all samples.

observed large similarities in population distribution within b-plaques and t-plaques. In detail, we found that the main cell populations are classical monocytes, macrophages, activated dendritic cells and plasmacytoid dendritic cells (Fig. 2a and b; Supplementary Fig. 11). When we analyzed CD45 $^+$ cells from carotid plaques, we identified PDC and aDC populations as main myeloid plaque components (Fig. 2a and b; Supplementary Fig. 12). We further investigated the event density distribution within the PDC populations in human carotid plaques. We identified 3 major areas of the vi-SNE map corresponding to peculiar PDC phenotypes that we classified as α, β and γ (Supplementary Fig. 12). PDC type-α represents a relatively small cluster with phagocytic and lipoprotein clearance predisposition due to high surface levels of scavenger receptors CD36, SRA-1 and CD14. PDC type-β is a larger cell cluster characterized by CD16^{high}, indicating a possible involvement in pro-inflammatory reactions. PDC type-γ appears to be exclusively specialized in lipid and lipoprotein uptake, provided the predominant surface expression levels of CD36 (Supplementary Fig. 12). Interestingly, in both bioengineered plaque models (b- and t-plaques) we identify PDC Type-β (Supplementary Fig. 11). Finally, we analyzed the gene expression profile of the CD45 $^+$ populations in ps-plaques and carotid plaques. We reported a significant down-regulation of pro-inflammatory and remodeling gene targets in carotid plaques compared to bioengineered plaques (Fig. 2c).

3.4. Low-density lipoprotein promotes the differentiation of a precursor myeloid population in biofabricated plaques

We investigated the effects of LDL on the differentiation of myeloid (CD45$^+$) subpopulations isolated from b- and t-plaques. To do so, we biofabricated ps-plaques using either the established protocol based on LDL-enriched medium or using LDL-free medium. We applied the vi-SNE workflow to compare the respective cell populations. In b-plaques we observed a reduced count of precursors in LDL-enriched versus LDL-free controls (p < 0.001, Fig. 3a, Supplementary Fig. 13) suggesting differentiation triggered by LDL. The difference in precursor counts can also be appreciated in the respective density plots (Fig. 3b, Supplementary Fig. 13). Additionally, we compared vi-SNE density plots from ps-plaques biofabricated in LDL-rich and LDL-free medium. To investigate variations in LDL triggered surface antigen expression within each population we overlapped the density plots with the marker expression level plot. We observed an LDL dependent density shift in aDC towards vi-SNE areas with CD11c^{high}, CD16^{high} and CD36^{high} expression levels (Fig. 3b and c). In t-plaques, we observed an LDL dependent density shift of M$_{φ1}$ towards CD36^{high} and CD11c^{high} areas of the vi-SNE map and of Mo$_{cl}$ towards a CD36^{high} vi-SNE area (Supplementary Fig. 14; Supplementary Fig. 15, Supplementary Fig. 16).

3.5. The hanging-drop environment allows the establishment of a pro-inflammatory niche

To uncover possible transcriptional effects exerted by LDL on key target genes, we investigated the expression profiles of the myeloid component during two steps of the ps-plaque biofabrication: (i) after 48 h in hanging-drop (T1) and (ii) at the end of the hanging-drop process (T2). We compared T1 and T2 from ps-plaques produced in LDL-free or LDL-enriched environment. Surprisingly, despite the induction of dendritic cell-specific intercellular adhesion molecule DC-SIGN (p < 0.001 versus p = 0.003, Fig. 4a) we did not find any significant LDL-dependent transcriptional change in b-plaques and t-plaques over time (Fig. 4a; Supplementary Fig. 17). On the other hand, we found that the hanging-drop process had, per se, a major influence on the gene expression levels by directly or

indirectly promoting the establishment of a pro-inflammatory environment. In detail, in b-plaques we observed a significant down-regulation of CCL26 (p < 0.001) and up-regulation of key pro-inflammatory genes CXCL10, CCR7 and IL23 (p < 0.001) during the transition from T1 to T2 and independently from the presence of LDL (Fig. 4a). We observed an indirect pro-inflammatory effect in t-plaques, exerted through the down-regulation of the anti-inflammatory cytokines CCL26, IL10 and CCL17 (p < 0.001, Supplementary Fig. 17). We validated these observations performing a control experiment in which we investigated the gene expression profile of CD45 $^+$ cells using a 2D co-culture approach (Supplementary Fig. 10a). As for the hanging drop approach, we performed the transcriptomic analysis over time (T1 and T2) in LDL-free and LDL-enriched medium, using both blood-derived and thp-1 cells (Supplementary Fig. 18). When we investigated the transcripts profile of blood-derived cells co-cultured in 2D we did not observe any time-dependent pro-inflammatory effect apart from the down-regulation of CD26 (p = 0.006 in LDL-rich condition; p < 0.001 in LDL-free condition). When we repeated the experiment using thp-1 co-cultured in 2D, not only we did not find any time-dependent pro-inflammatory effect but also we reported a significant time-dependent anti-inflammatory effect achieved with the down-regulation of two pro-inflammatory markers: PTGS1 and ALOX5 (both p < 0.001, Supplementary Fig. 18).

3.6. Low-density lipoprotein enhances cell death in ps-plaques biofabricated with primed blood cells

To further explore the effects of LDL on the ps-plaque model we conducted a bivalent analysis. First, we investigated the cell viability within the ps-plaque. We measured and compared the ATP levels produced by the biofabricated plaques in LDL-enriched and LDL-free medium. We did not find any significant LDL-dependent differences in ATP levels in either b- or t-plaques (Fig. 4b). However, we observed a general tendency of lower ATP levels in plaques produced in LDL-rich environments. We then measured the necrotic area at the circular cross-section and we found that b-plaques fabricated in presence of LDL had a significantly larger necrotic area in comparison to their LDL-free counterparts, suggesting an LDL-dependent necrotic effect (p < 0.001, Fig. 4d and e). Second, we investigated differences in plaque dimensions to verify possible effects of LDL on cell proliferation. We found no difference in circular cross-section area — consequently in size — of LDL-enriched vs LDL-free plaques (Fig. 4c).

4. Discussion

With the biofabrication of the ps-plaque we aimed at replicating cellular architecture and extracellular microenvironment of a human atherosclerotic plaque to close an open modeling gap in the field of atherosclerosis research. It has been described that the fibroatheroma cellular composition is mainly characterized by macrophages and dendritic cells retaining pro-inflammatory and remodeling abilities [19–21]. To achieve plaque cell populations as similar as possible to human atherosclerotic plaque phenotypes we established a differentiation-priming protocol based on a mild LPS stimulation of cultured adhesive myeloid cells [22,23]. To visualize and quantify the effects of this procedure on cell population remodeling we used the vi-SNE workflow [18,24,25]. With this strategy we identified a total of 15 cell populations, differently distributed among samples. We were able to classify these populations according to the prevalence of specific surface markers [26,27]. We were also able to track intra-population density shifts and changes in numbers of events. The sensitivity of the vi-SNE analysis allowed the identification of under-represented myeloid
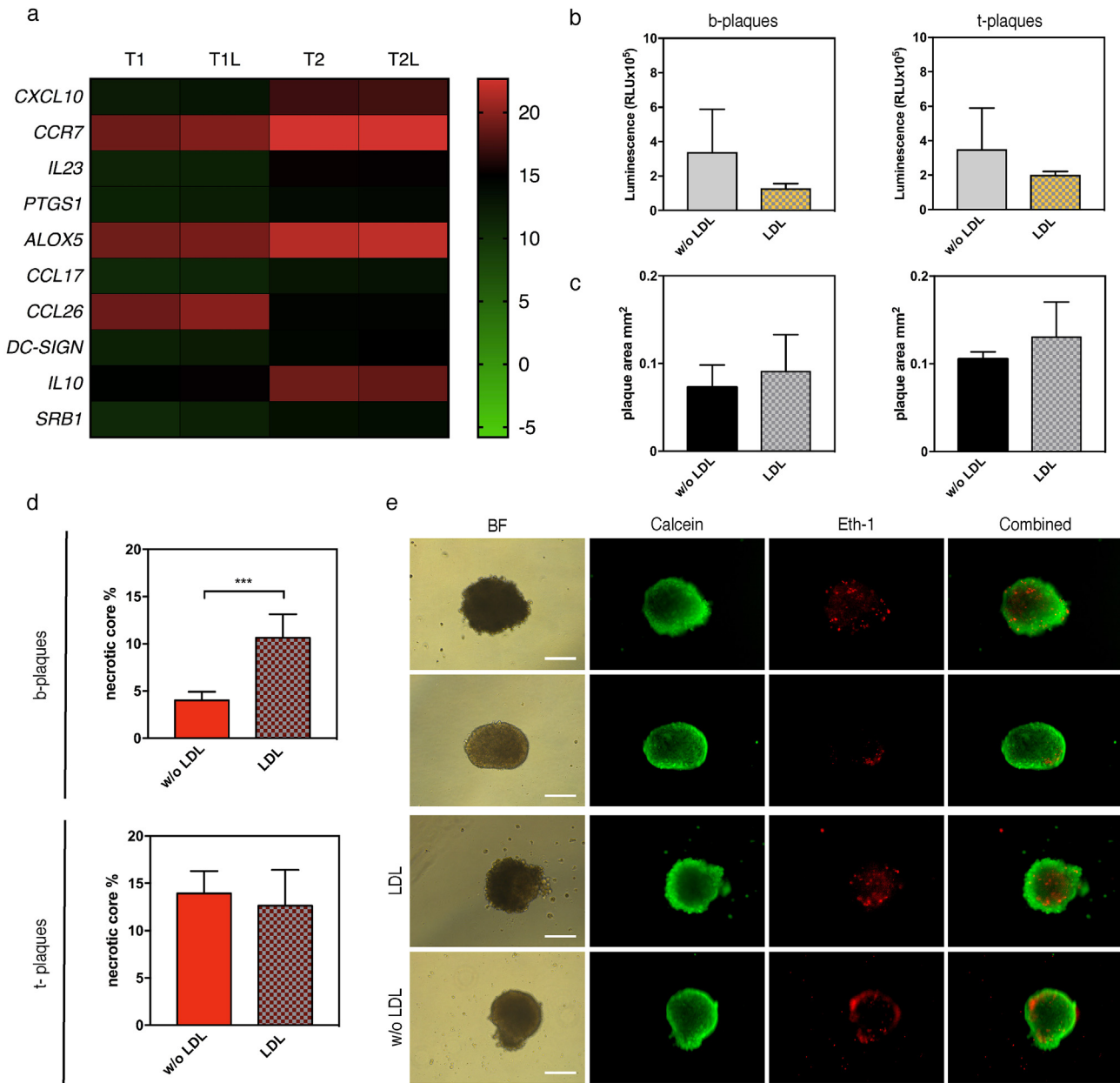
Fig. 4. **Transcript analysis of pro- and anti-inflammatory gene targets in b-plaques and LDL effects on cell viability and plaque dimension.** (a) Heat-map indicating the expression levels of target genes of interest at T1 and T2 of b-plaque formation in LDL presence (T1L, T2L) or absence (T1, T2). Expression levels are reported in ΔCt over the mean of the housekeeping genes GAPDH and 18S; n = 5. (**b**) ATP levels, indicated in relative luminescence units (RLU), were measured and compared in b- and t-plaques; n = 5. (**c**) Plaque circular cross-section area (mm²) as indicator of plaque dimension; n = 5. (**d**−**e**) The ps-plaque necrotic area was measured at the circular cross-section at the great circle of the spheroid, and indicated as percentage over alive cells. Living cells (green) are stained with calcein while dead cells (red) with Eth-1; n = 5, ***p < 0.001, scale bar 100 μm.

populations, otherwise difficult to identify with commonly used flow cytometry analysis tools. Thanks to the vi-SNE workflow we identified in blood-derived myeloid samples both plasmacytoid dendritic cells (PDC) and pre-classical dendritic cells (pre-cDCs) [27].

The vi-SNE analysis reported a yet unidentified myeloid population in both thp-1 and blood derived samples. We observed a significant decrease of this population upon differentiation-priming treatment in both blood-derived and thp-1 samples. The decrease was concomitant to a significant increase in pre-cDC count in blood-derived samples and to an increase in PDC in thp-1 samples. Based on the current myeloid differentiation map [19,27] and on our observations we propose that the yet unidentified

population could be classified as a circulating common precursor of pre-cDC and PDC, differentiating from the common dendritic cell precursors located in the bone marrow (Supplementary Fig. 19). Further investigation on this cell population could improve understanding and redesigning of the myeloid differentiation map.

Primed cells and myofibroblasts were used for ps-plaque biofabrication and were combined to generate a stratified cell-spheroid with myofibroblasts located at the periphery and a compact, collagenous and lipid-rich core of CD45 + cells. We sorted and compared the CD45 + populations derived from ps-plaques and native human carotid plaques using qPCR and the vi-SNE workflow. First, we compared the gene expression of CD45 + cells isolated from ps-plaques and native plaques and we reported major

differences in transcripts level. Second, we investigated and compared the cell populations between ps-plaques and native plaques and we found that PDC and activated dendritic cells (aDC) are the main myeloid component of thin-cap stage atherosclerotic plaques. This finding is *per se* surprising provided that macrophages and macrophage-derived foam cells are thought to be the main cellular component of atherosclerotic lesions, at least in early developmental stages, as discussed by Moore and Randolph [28,29]. Importantly, both PDC and aDC are present in the biofabricated models although in low percentages. It is possible that the differences found in both gene expression and cell composition when comparing ps-plaques and carotid plaques are due to differences in the temporal and developmental stages of both plaque types.

Bonanno et al. previously analyzed the cell component of human carotid plaques using flow cytometry showing that about 17% of the lesion (considering cells of lymphoid and myeloid origin and smooth muscle cells) is constituted by CD68 $^+$ cells [30]. They also reported that about 40% of the cells within the plaque expressed MHC class II molecules (HLA-DR+) suggesting that these populations could act as antigen-presenting cells [30]. It was also proven that early-committed immature DCs are positive for CD68 and HLA-DR markers [31], supporting the idea that the cells analyzed by Bonanno et al. might have been in part PDC and activated dendritic cells. Additionally, it is known that PDC aggravate atherosclerotic lesion formation and that their depletion reduces aortic plaque growth by 46% in *Apoe$^{-/-}$* mice [32,33]. PDC are also able to uptake oxidized LDL (ox-LDL) *ex vivo*, and promote PDC-driven antigen-specific T-cell proliferation [32]. Finally, it was reported that PDC function and cytokine release is impaired in patients suffering from coronary artery disease [34,35]. Taken together, these discoveries are in line with our findings and might change the scenario of future atherosclerosis treatments.

Within the PDC population we identified 3 overrepresented sub-populations that we named type-α, type- β and type-γ. We observed that these subpopulations retain some degree of specialization due to differential marker expression levels. This difference could be the basis of a differential contribution to plaque maturation. For instance, PDC type-α display surface marker expression levels (CD36^{high}, CD14^{high} and SRA-1^{high}) of a specialized scavenger population [36]. With the ps-plaque model we were able to investigate LDL effects on intra-plaque population remodeling and cell viability. In detail, we monitored LDL-dependent event density shift within the PDC population towards PDC type-β phenotype. This shift was not concomitant with the increase in the PDC count implying a PDC polarization towards CD36^{high} and CD16^{high} vi-SNE regions and indicating a possible LDL-triggered acquisition from PDC of scavenger and pro-inflammatory phenotype. Additionally, we found that LDL presence during ps-plaque formation significantly decreased the count of dendritic precursors in both b- and t-plaques and triggered the polarization of aDCs towards CD11c^{high}, CD16^{high} and CD36^{high} levels. These findings are supported by the previous observations that LDL and mildly oxidized LDL affect DC maturation and promote pro-inflammatory function [37–39].

We observed an LDL-dependent decrease of plaque cell viability in b-plaques but not in t-plaques. It was shown that LDL and ox-LDL accumulate in the cytoplasm of the phagocyte and ultimately contribute to a deregulation of lipid metabolism by activating the unfolded protein response (UPR), leading to cell death [40]. The non-significant decrease in cell viability observed in t-plaques might be due to intrinsic differences in population counts among ps-plaque types. In fact, t-plaques show higher intermediate monocyte counts when compared to b-plaques. Furthermore, b-plaques display a larger population of activated dendritic cells

compared to t-plaques. In summary, t-plaques are constituted by a more immature cellular milieu compared to b-plaques. For this reason we hypothesize that populations within t-plaques would require more time to develop towards a death-susceptible stage in presence of LDL.

We investigated time-dependent effects of LDL on the expression profile of myeloid cells within the biofabricated plaque. We found no significant difference in transcript levels of selected pro-inflammatory and remodeling target genes [41] comparing LDL-rich and LDL-free plaques. LDL effects on myeloid cell transcriptome were previously investigated by exposing the cells directly in contact with modified forms of LDL and not by directly testing native lipoproteins [42,43]. However, native LDL might retain slower time of action at the transcriptomic level compared to its modified counterparts, as previously observed [44]. Interestingly, we detected time-dependent gene induction leading to pro-inflammatory cell phenotype independently from LDL treatment. The latter was either prompted by direct up-regulation of pro-inflammatory target genes in b-plaques (*CXCL10, CCR7, IL23, PTGS1*) or indirectly triggered by down-regulation of anti-inflammatory genes in t-plaques (*CCL17, CCL26, IL10*). It was recently shown that three-dimensional spheroid cultures of adipose-derived mesenchymal stem cells (MSC) enhance protein levels of the anti-inflammatory tumor necrosis factor alpha stimulated gene/protein 6 (TGS-6) [45]. On the other hand, the study conducted by Bartosh et al. did not include any test to verify the possible concomitant release of pro-inflammatory proteins, leaving an unanswered question open for further investigations.

In conclusion, the ps-plaque is assembled with myeloid cell populations that are shared with human native plaques. These cells are embedded in a collagenous and lipid-rich extracellular matrix surrounded by a fibrotic layer. To our knowledge the ps-plaque can be considered the *in vitro* model closer to human fibroatheroma available up to date. Importantly, the present model has the major limitation to not consider sex, age and genetic predisposition, which, are in fact, key factors influencing plaque initiation and development. In addition, the current model is lacking B and T lymphocytes that might provide and important contribution in exacerbating inflammation at the plaque level. However, the participation of cells from the adaptive immune system to plaque development is still under debate [46,47]. In terms of acellular components the model is missing calcification deposits, often encountered in late-stage plaques. Despite the absence of calcified areas, calcification is per-se not a predictor of unstable plaques (vulnerable plaques) that are prone to rupture and to initiate ischemic events [48]. The intra-plaque calcification mechanisms are tightly regulated by monocyte/macrophages residing within the plaque [49]. In this regard the 3D plaque model could serve as basis for both (i) further investigations aimed at uncovering the mechanisms driving calcium deposition within the atheroma and (ii) for the biofabrication of more complex and diversified plaque models mimicking different stages of atherosclerosis and peculiar plaque composition.

Despite the ps-plaque model alone cannot address the complexity of the human vascular environment in which wall shear stress, circulating innate and adaptive immune cells and variations in LDL cholesterol, blood pressure and diabetes, play a pivotal role in modulating plaque development, it provides a tool for investigating cellular interplay, viability, metabolism and behavior in a confined environment sharing anatomopathological features with human native plaques. The miniaturized plaque can be integrated in a 96-well or 384-well platform and used for drug design and screening purposes. Additionally, it can be employed for increasing the basic understanding of late-stage atherosclerosis disease phenomena including possible anti-inflammatory/atheroprotective

role of HDL, plaque calcification and rupture or can be integrated in more complex bioengineered dynamic systems, improving existing tissue engineered vascular atherosclerosis models [14]. Finally, the biofabrication process can be applied to blood-derived myeloid cells isolated from patients with different causative mutations of familial hypercholesterolemia (FH, life threatening athero-prone genetic disorder) in order to produce autologous FH-3D models to identify mutation-dependent differences in plaque architecture, cellular composition, cell metabolism and viability, with the aim of predicting mutation-dependent disease prognosis.

Conflicts of interest

The authors declare no competing financial interest.

Author contributions

A.M. conceived the project and designed the experiments. A.M. and C.S. established and performed the hanging drop culture experiments. A.M. performed the qPCR, flow cytometry and viability assays and analyzed the data. Funding for the project were provided by A.v.E., S.P.H. and B.W.. A.M. wrote the manuscript with the contribution of C.S., A.v.E., S.P.H. and B.W..

Acknowledgements

Appendix A. Supplementary data

Supplementary data related to this article can be found at https://doi.org/10.1016/j.biomaterials.2017.09.034.

References

[1] J.L. Goldstein, M.S. Brown, A century of cholesterol and coronaries: from plaques to genes to statins, Cell 161 (1) (2015) 161—172.

[2] A. von Eckardstein, Is there a need for novel cardiovascular risk factors? Nephrol. Dial. Transplant. 19 (4) (2004) 761—765.

[3] J.M. Kelm, M.Y. Emmert, A. Zurcher, D. Schmidt, Y. Begus Nahrmann, K.L. Rudolph, B. Weber, C.E. Brokopp, T. Frauenfelder, S. Leschka, B. Odermatt, R. Jenni, V. Falk, G. Zund, S.P. Hoerstrup, Functionality, growth and accelerated aging of tissue engineered living autologous vascular grafts, Biomaterials 33 (33) (2012) 8277—8285.

[4] K. Yahagi, F.D. Kolodgie, F. Otsuka, A.V. Finn, H.R. Davis, M. Joner, R. Virmani, Pathophysiology of native coronary, vein graft, and in-stent atherosclerosis, Nat. Rev. Cardiol. 13 (2) (2016) 79—98.

[5] J.F. Bentzon, F. Otsuka, R. Virmani, E. Falk, Mechanisms of plaque formation and rupture, Circ. Res. 114 (12) (2014) 1852—1866.

[6] R. Virmani, A.P. Burke, F.D. Kolodgie, A. Farb, Pathology of the thin-cap fibroatheroma: a type of vulnerable plaque, J. Interv. Cardiol. 16 (3) (2003) 267—272.

[7] J.D. Smith, E. Trogan, M. Ginsberg, C. Grigaux, J. Tian, M. Miyata, Decreased atherosclerosis in mice deficient in both macrophage colony-stimulating factor (op) and apolipoprotein E, Proc. Natl. Acad. Sci. U. S. A. 92 (18) (1995) 8264—8268.

[8] Y. Kojima, J.P. Volkmer, K. McKenna, A.J. Lusis, C.L. Miller, D. Direnzo, V. Nanda, J. Ye, A.J. Connolly, E.E. Schadt, T. Quertermous, P. Betancur, L. Maegdefessel, L.P. Matic, U. Hedin, I.L. Weissman, N.J. Leeper, CD47-blocking antibodies restore phagocytosis and prevent atherosclerosis, Nature 536 (7614) (2016) 86—90.

[9] C.A. Reardon, L. Blachowicz, J. Lukens, M. Nissenbaum, G.S. Getz, Genetic background selectively influences innominate artery atherosclerosis: immune system deficiency as a probe, Arterioscler. Thromb. Vasc. Biol. 23 (8) (2003) 1449—1454.

[10] J.K. Williams, M.L. Armstrong, D.D. Heistad, Vasa vasorum in atherosclerotic coronary arteries: responses to vasoactive stimuli and regression of atherosclerosis, Circ. Res. 62 (3) (1988) 515—523.

[11] M.L. Armstrong, M.B. Megan, Lipid depletion in atheromatous coronary arteries in rhesus monkeys after regression diets, Circ. Res. 30 (6) (1972) 675—680.

[12] D.J. Graham, J.J. Alexander, R. Miguel, Aortic endothelial and smooth muscle cell co-culture: an *in vitro* model of the arterial wall, J. Invest. Surg. 4 (4) (1991) 487—494.

[13] M. Navab, G.P. Hough, L.W. Stevenson, D.C. Drinkwater, H. Laks, A.M. Fogelman, Monocyte migration into the subendothelial space of a coculture of adult human aortic endothelial and smooth muscle cells, J. Clin. Invest. 82 (6) (1988) 1853—1863.

[14] J. Robert, B. Weber, L. Frese, M.Y. Emmert, D. Schmidt, A. von Eckardstein, L. Rohrer, S.P. Hoerstrup, A three-dimensional engineered artery model for *in vitro* atherosclerosis research, PLos One 8 (11) (2013) e79821.

[15] B. Dorweiler, M. Torzewski, M. Dahm, V. Ochsenhirt, H.A. Lehr, K.J. Lackner, C.F. Vahl, A novel *in vitro* model for the study of plaque development in atherosclerosis, Thromb. Haemost. 95 (1) (2006) 182—189.

[16] K. Menck, D. Behme, M. Pantke, N. Reiling, C. Binder, T. Pukrop, F. Klemm, Isolation of human monocytes by double gradient centrifugation and their differentiation to macrophages in teflon-coated cell culture bags, J. Vis. Exp. 91 (2014) e51554.

[17] L. Van Der Maaten, G. Hinton, Visualizing high-dimensional data using t-sne. journal of machine learning research, J. Mach. Learn Res. 9 (2008) 26.

[18] A.D. Amir el, K.L. Davis, M.D. Tadmor, E.F. Simonds, J.H. Levine, S.C. Bendall, D.K. Shenfeld, S. Krishnaswamy, G.P. Nolan, D. Pe'er, viSNE enables visualization of high dimensional single-cell data and reveals phenotypic heterogeneity of leukemia, Nat. Biotechnol. 31 (6) (2013) 545—552.

[19] M.I. Cybulsky, C. Cheong, C.S. Robbins, Macrophages and dendritic cells: partners in atherogenesis, Circ. Res. 118 (4) (2016) 637—652.

[20] G. Chinetti-Gbaguidi, S. Colin, B. Staels, Macrophage subsets in atherosclerosis, Nat. Rev. Cardiol. 12 (1) (2015) 10—17.

[21] K.J. Moore, F.J. Sheedy, E.A. Fisher, Macrophages in atherosclerosis: a dynamic balance, Nat. Rev. Immunol. 13 (10) (2013) 709—721.

[22] F. Awad, E. Assrawi, C. Jumeau, S. Georgin-Lavialle, L. Cobret, P. Duquesnoy, W. Piterboth, L. Thomas, K. Stankovic-Stojanovic, C. Louvrier, I. Giurgea, G. Grateau, S. Amselem, S.A. Karabina, Impact of human monocyte and macrophage polarization on NLR expression and NLRP3 inflammasome activation, PLos One 12 (4) (2017), e0175336.

[23] M. Peters, K. Dudziak, M. Stiehm, A. Bufe, T-cell polarization depends on concentration of the danger signal used to activate dendritic cells, Immunol. Cell Biol. 88 (5) (2010) 537—544.

[24] S. Van Gassen, B. Callebaut, M.J. Van Helden, B.N. Lambrecht, P. Demeester, T. Dhaene, Y. Saeys, FlowSOM: using self-organizing maps for visualization and interpretation of cytometry data, Cytom. A 87 (7) (2015) 636—645.

[25] H. Chen, M.C. Lau, M.T. Wong, E.W. Newell, M. Poidinger, J. Chen, Cytofkit: a bioconductor package for an integrated mass cytometry data analysis pipeline, PLoS Comput. Biol. 12 (9) (2016), e1005112.

[26] J. Yang, L. Zhang, C. Yu, X.F. Yang, H. Wang, Monocyte and macrophage differentiation: circulation inflammatory monocyte as biomarker for inflammatory diseases, Biomark. Res. 2 (1) (2014) 1.

[27] F. Geissmann, M.G. Manz, S. Jung, M.H. Sieweke, M. Merad, K. Ley, Development of monocytes, macrophages, and dendritic cells, Science 327 (5966) (2010) 656—661.

[28] K.J. Moore, I. Tabas, Macrophages in the pathogenesis of atherosclerosis, Cell 145 (3) (2011) 341—355.

[29] G.J. Randolph, Mechanisms that regulate macrophage burden in atherosclerosis, Circ. Res. 114 (11) (2014) 1757—1771.

[30] E. Bonanno, A. Mauriello, A. Partenzi, L. Anemona, L.G. Spagnoli, Flow cytometry analysis of atherosclerotic plaque cells from human carotids: a validation study, Cytometry 39 (2) (2000) 158—165.

[31] K. Kishimoto, G. Tate, G. Kitamura, M. Kojima, T. Mitsuya, Cytologic features and frequency of plasmacytoid dendritic cells in the lymph nodes of patients with histiocytic necrotizing lymphadenitis (Kikuchi-Fujimoto disease), Diagn. Cytopathol. 38 (7) (2010) 521—526.

[32] Y. Doring, H.D. Manthey, M. Drechsler, D. Lievens, R.T. Megens, O. Soehnlein, M. Busch, M. Manca, R.R. Koenen, J. Pelisek, M.J. Daemen, E. Lutgens, M. Zenke, C.J. Binder, C. Weber, A. Zernecke, Auto-antigenic protein-DNA complexes stimulate plasmacytoid dendritic cells to promote atherosclerosis, Circulation 125 (13) (2012) 1673—1683.

[33] N. Macritchie, G. Grassia, S.R. Sabir, M. Maddaluno, P. Welsh, N. Sattar, A. Ialenti, M. Kurowska-Stolarska, I.B. McInnes, J.M. Brewer, P. Garside, P. Maffia, Plasmacytoid dendritic cells play a key role in promoting atherosclerosis in apolipoprotein E-deficient mice, Arterioscler. Thromb. Vasc. Biol. 32 (11) (2012) 2569—2579.

[34] I. Van Brussel, E.A. Van Vre, G.R. De Meyer, C.J. Vrints, J.M. Bosmans, H. Bult, Decreased numbers of peripheral blood dendritic cells in patients with coronary artery disease are associated with diminished plasma Flt3 ligand levels and impaired plasmacytoid dendritic cell function, Clin. Sci. (Lond.) 120 (9) (2011) 415—426.

[35] J.J. Corrales, M. Almeida, R.M. Burgo, P. Hernandez, J.M. Miralles, A. Orfao, Decreased production of inflammatory cytokines by circulating monocytes and dendritic cells in type 2 diabetic men with atherosclerotic complications, J. Diabetes Complicat. 21 (1) (2007) 41—49.

[36] V.V. Kunjathoor, M. Febbraio, E.A. Podrez, K.J. Moore, L. Andersson, S. Koehn, J.S. Rhee, R. Silverstein, H.F. Hoff, M.W. Freeman, Scavenger receptors class A-I/II and CD36 are the principal receptors responsible for the uptake of modified low density lipoprotein leading to lipid loading in macrophages, J. Biol. Chem. 277 (51) (2002) 49982—49988.

[37] R. Zaguri, I. Verbovetski, M. Atallah, U. Trahtemberg, A. Krispin, E. Nahari, E. Leitersdorf, D. Mevorach, 'Danger' effect of low-density lipoprotein (LDL) and oxidized LDL on human immature dendritic cells, Clin. Exp. Immunol. 149 (3) (2007) 543—552.

[38] C.J. Alderman, P.R. Bunyard, B.M. Chain, J.C. Foreman, D.S. Leake, D.R. Katz, Effects of oxidised low density lipoprotein on dendritic cells: a possible immunoregulatory component of the atherogenic micro-environment? Cardiovasc Res. 55 (4) (2002) 806—819.

[39] L. Perrin-Cocon, F. Coutant, S. Agaugue, S. Deforges, P. Andre, V. Lotteau, Oxidized low-density lipoprotein promotes mature dendritic cell transition from differentiating monocyte, J. Immunol. 167 (7) (2001) 3785—3791.

[40] B. Feng, P.M. Yao, Y. Li, C.M. Devlin, D. Zhang, H.P. Harding, M. Sweeney, J.X. Rong, G. Kuriakose, E.A. Fisher, A.R. Marks, D. Ron, I. Tabas, The endoplasmic reticulum is the site of cholesterol-induced cytotoxicity in macrophages, Nat. Cell Biol. 5 (9) (2003) 781—792.

[41] F.O. Martinez, S. Gordon, M. Locati, A. Mantovani, Transcriptional profiling of the human monocyte-to-macrophage differentiation and polarization: new molecules and patterns of gene expression, J. Immunol. 177 (10) (2006) 7303—7311.

[42] S. Bekkering, J. Quintin, L.A. Joosten, J.W. van der Meer, M.G. Netea, N.P. Riksen, Oxidized low-density lipoprotein induces long-term proinflammatory cytokine production and foam cell formation via epigenetic reprogramming of monocytes, Arterioscler. Thromb. Vasc. Biol. 34 (8) (2014) 1731—1738.

[43] L.J. van Tits, R. Stienstra, P.L. van Lent, M.G. Netea, L.A. Joosten, A.F. Stalenhoef, Oxidized LDL enhances pro-inflammatory responses of alternatively activated M2 macrophages: a crucial role for Kruppel-like factor 2, Atherosclerosis 214 (2) (2011) 345—349.

[44] S. Damian-Zamacona, P. Toledo-Ibelles, M.Z. Ibarra-Abundis, L. Uribe-Figueroa, E. Hernandez-Lemus, K.P. Macedo-Alcibia, B. Delgado-Coello, J. Mas-Oliva, J.P. Reyes-Grajeda, Early transcriptomic response to LDL and oxLDL in human vascular smooth muscle cells, PLos One 11 (10) (2016) e0163924.

[45] T.J. Bartosh, J.H. Ylostalo, A. Mohammadipoor, N. Bazhanov, K. Coble, K. Claypool, R.H. Lee, H. Choi, D.J. Prockop, Aggregation of human mesenchymal stromal cells (MSCs) into 3D spheroids enhances their antiinflammatory properties, Proc. Natl. Acad. Sci. U. S. A. 107 (31) (2010) 13724—13729.

[46] H.M. Dansky, S.A. Charlton, M.M. Harper, J.D. Smith, T and B lymphocytes play a minor role in atherosclerotic plaque formation in the apolipoprotein E-deficient mouse, Proc. Natl. Acad. Sci. U. S. A. 94 (9) (1997) 4642—4646.

[47] F. Cheng, L. Twardowski, K. Reifenberg, K. Winter, A. Canisius, E. Pross, J. Fan, E. Schmitt, L.D. Shultz, K.J. Lackner, M. Torzewski, Combined B, T and NK cell deficiency accelerates atherosclerosis in BALB/c mice, PLos One 11 (8) (2016) e0157311.

[48] F. Otsuka, K. Sakakura, K. Yahagi, M. Joner, R. Virmani, Has our understanding of calcification in human coronary atherosclerosis progressed? Arterioscler. Thromb. Vasc. Biol. 34 (4) (2014) 724—736.

[49] Y. Tintut, J. Patel, M. Territo, T. Saini, F. Parhami, L.L. Demer, Monocyte/macrophage regulation of vascular calcification *in vitro*, Circulation 105 (5) (2002) 650—655.